Comptes Rendus
Mécanique
0000, 1, nº 0, p. 000-000
DOI unassigned yet

On three-dimensional bluff body wake symmetry breaking with free-stream turbulence and residual asymmetry

Olivier Cadot[*, a], **Maha Almarzooqi**[a, b], **Antoine Legeai**[a, c], **Vladimir Parezanović**[b] **and Luc Pastur**[c]

[a] School of Engineering, University of Liverpool, Liverpool L69 3GH, UK.

[b] Khalifa University of Science and Technology, P.O. Box 127788, Abu Dhabi, UAE.

[c] IMSIA-ENSTA ParisTech, 828 Bd des Maréchaux F-91762 Palaiseau, France.

E-mail: cadot@liverpool.ac.uk (0.Cadot).

Abstract. The paper reports on the bi-stable turbulent wake dynamics of a three-dimensional bluff body. It is shown that the occurrence of the switching between the two wake states decreases as the turbulent intensity of the incoming flow is made larger by an additional upstream grid. A detailed analysis of the jumps statistics indicates that the turbulent fluctuation of each wake state is also decreased. It is concluded that the states switching is thus triggered by large fluctuations produced by the wake instabilities and not by those of the incoming flow. It is also shown that increasing the free-stream turbulence intensity reinforces the permanent asymmetry of each state and increases the wake sensitivity to residual asymmetries.

Keywords. Turbulence, Instability, Aerodynamics, Analogy.

Mathematical subject classification (2010). 00X99.

This article is a draft (not yet accepted!)

1. Introduction

Analogies in physics are a source of inspiration to pave the way of understanding intricate phenomena. The elegant and original experimental research work of Yves Couder is often built on the basis of clever analogies, such as the use of ferromagnetic interaction to explain the self-organisation into Fibonacci series in plants [1], the observation of a pattern of cracks formed in gel to model leaf venation [2] or to study the behaviour of bouncing drops to tackle quantum mechanics [3, 4]. The research paper we present is not exploiting an analogy as in these cited works, but we wished to introduce our original contribution by mentioning a possible analogy as a tribute to Yves.

* Corresponding author.

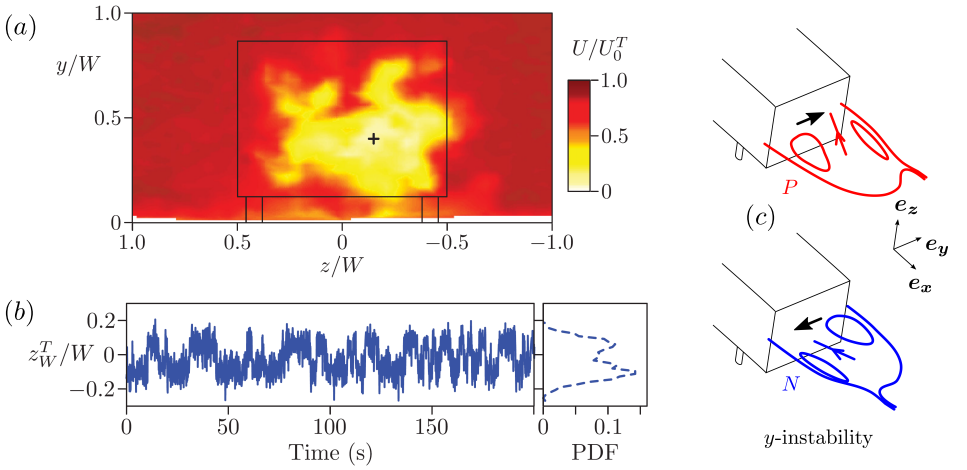

Figure 1. Figures extracted from [5, 6] about the turbulent wake of a squareback body at $\mathrm{Re} \sim 10^5$ showing the instantaneous streamwise velocity field with a laterally deflected wake on the right hand-side (*a*) and the motion of the deflected position with corresponding statistics (*b*). Schematic drawing of the two wake states denoted P and N with their associated base pressure gradient (*c*).

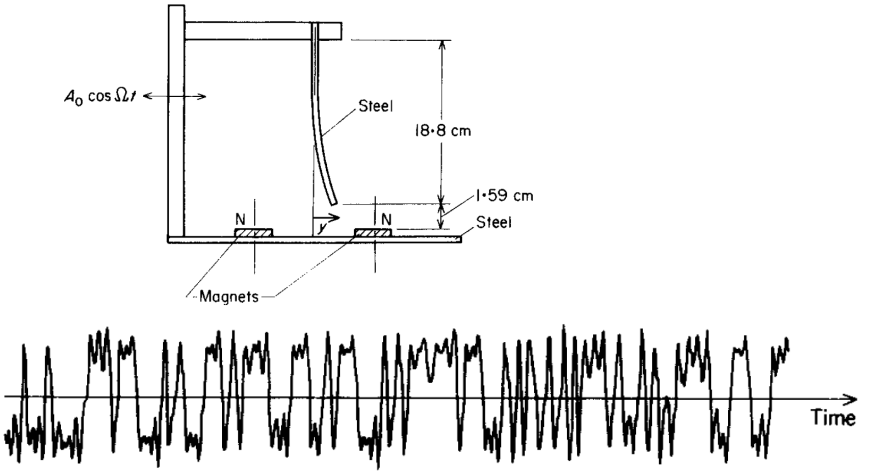

Figure 2. Figures extracted from [9] showing the experimental apparatus of a cantilevered ferroelastic beam buckled using two permanent magnet and chaotic response of the deflection angle under the periodic forcing.

The recent observations of turbulent wake dynamics from rectangular base bluff bodies report on the switching dynamics between two very distinctive global states of the wake [5, 6]. Each wake state is breaking the symmetry on timescales much longer than the convective timescale as illustrated in Fig. 1. As a result, the turbulent wake is permanently asymmetric. This global asymmetry is reminiscent of the first bifurcation commonly developed by three-dimensional bodies during the laminar regime [5, 7, 8] leading to a steady symmetry breaking. This pitchfork bifurcation is equivalent to the buckling instability observed in solids. The striking analogy can

be seen by comparing the deflection of the turbulent wake (Fig. 1*b*) and the deflection angle of the buckled beam in the experiment of [9] illustrated in Fig. 2. While the sensitivity to initial conditions is clearly responsible for the random response of the beam, the wake dynamics involve more complex physics due to space-time turbulent fluctuations. However, low order modelling of the wake using a stochastic approach [10] is successful in retrieving the dynamics of the turbulent wake deflection with a double-well potential in a Langevin equation [11]. The question is what is the origin of the stochastic term and how is it related to the turbulent intensity in the incoming flow or to the wake unsteadiness. To address this issue, the paper investigates experimentally the occurrence of the wake switching for different free-stream turbulent intensities considering also residual asymmetries produced by yawing the model.

In the following, the experimental set-up is detailed in § 2 and the results shown in two parts are presented in § 3. The first part § 3.1 investigates how residual asymmetries affect the wake switching statistics and the second part § 3.2 focuses on the effect of the free-stream turbulent intensity. Results are discussed and concluded in § 4.

2. Experimental set-up

The model is presented in Fig. 3(*a*). It has a total length of $2.5H$, a base aspect ratio of $W/H = 4/3$ and a ground clearance of $0.15H$ with $H = 60$ mm. It is supported with a central NACA profile instead of the four cylinders as classically used for studies in the context of ground vehicle aerodynamics [12]. The yaw β is adjusted by rotating together the model and the NACA profile. There are four pressure taps at the body base to measure the 2 components of the non-dimensional base pressure gradients g_y and g_z expressed as the pressure coefficient differences divided by the separating distance in H unit [13]. The pressure is measured using a Scanivalve pressure scanner ZOC33 connected through one meter long vinyl tubes to each pressure tap. Due to the low pass filtering introduced by the tubing, the dynamical response is limited to about 50 Hz, but that is sufficient for the present study.

The wind tunnel has a 300×300 mm cross section with a natural free-stream turbulence intensity of 1.8% that can be increased to 5.6% by placing the additional upstream grid shown in Fig. 3(*a*). The grid is composed of rods, $d = 3$ mm in diameter, arranged in square meshes of size $M = 19$ mm giving a solidity $\sigma = \frac{d}{M}(2 - \frac{d}{M}) = 0.29$. Both free-stream turbulent intensities have been measured at the location of the model (vertical dashed line in Fig. 3*a*) with $U_\infty = 20$ m.s^{-1} using a single hot wire anemometer from DANTEC. The power spectrum of the free-stream velocity is shown without and with the grid in Fig. 3(*b*). When the body is installed, and the velocity set to $U_\infty = 20$ m.s^{-1}, the flow Reynolds number is $\mathrm{Re}=\frac{U_\infty H}{\nu} \approx 80{,}000$ for both free-streams.

Two series of experiments with the different free-stream turbulent intensities of 1.8% and 5.6% are conducted changing the body yaw β from $-2°$ to $+2°$ in steps of $0.5°$. For each yaw angle, pressures are recorded at a sampling frequency of 1 kHz during $T = 10$ minutes or equivalently during $TU_\infty/H = 200 \times 10^3$ in non-dimensional time units. As a reminder, a natural large-scale characteristic time for the three-dimensional turbulent wake is the period of vortex shedding $1/f_s$ commonly observed for a Strouhal number $\mathrm{St}= f_s H/U_\infty \approx 0.2$ [13, 14], which in non-dimensional time units gives 5. All pressure data are low pass filtered with a cut-off frequency of $f_{\text{cut-off}} = 15$ Hz, equivalent to $\mathrm{St}_{\text{cut-off}} = 0.045$. The dynamics studied in the work thus involve a very long timescale, much larger than the characteristic time for vortex shedding.

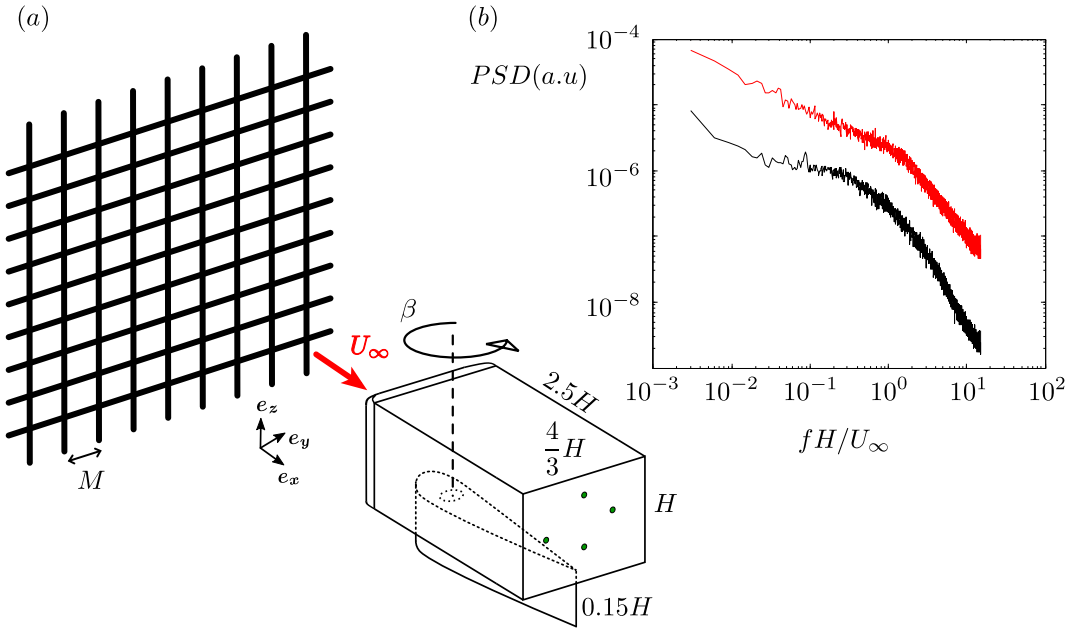

Figure 3. Experimental set-up (*a*) showing the grid placed $5H$ upstream the fore-body. The four pressure measurements are displayed by the four dots at the base. Velocity power spectrum (*b*) of the free-stream at the body location (dashed vertical line in *a*) with (red) and without (black) the grid. The free-stream turbulent intensity are $T.I.$ = 5.6% with the grid and $T.I.$ = 1.8% without the grid.

3. Results

3.1. *Asymmetry effects on switching statistics*

We first consider the wake dynamics with the lower turbulent intensity. Time series of the horizontal pressure gradient g_y are shown in Fig. 4 for the body aligned with the wind in Fig. 4(*a*) and with a yaw $\beta = -2°$ in Fig. 4(*b*). The two states denoted P and N (for positive and negative gradient) are clearly observable around +0.1 and −0.1. Events of zero horizontal gradient are indicated with red vertical segments and could either correspond in Fig. 4(*a*) to a clear switching between the two states (as around $tU_\infty H \simeq 1000$), or switching attempts (as observed around 1500), or simply a large turbulent fluctuation (likely observed at 3500). While the switching does correspond to a large scale or global change of the wake from one state to the other, the turbulent fluctuation only reflects a local pressure fluctuation. Similar events are also observed for the body in yaw in Fig. 4(*b*) but with a clear predominance of the N states. The waiting times statistics between two consecutive events $g_y = 0$ are displayed in Fig. 4(*c*) for the two cases $\beta = 0°$ and $\beta = -2°$. Despite the limited convergence of the data, we can see similar statistics at small waiting times while the yawed case shows more events of longer waiting time. The mean switching rate per non-dimensional time unit $\mathcal{N}_{(g_y=0)}$, given by the inverse of the mean waiting time, is then larger for the body aligned, $\mathcal{N}_{(g_y=0)} = 7.2 \times 10^{-3}$ than for the body in yaw $\mathcal{N}_{(g_y=0)} = 3.7 \times 10^{-3}$.

The probability density functions (PDF) of the pressure gradient components are shown in Fig. 5 for the two body alignments. The bi-modal shape of the $PDF(g_y)$ associated with two most probable gradient values reflects the two states. In order to characterize the turbulent fluctuation around each state, we realise Gaussian best fits centred on the two most probable gradients,

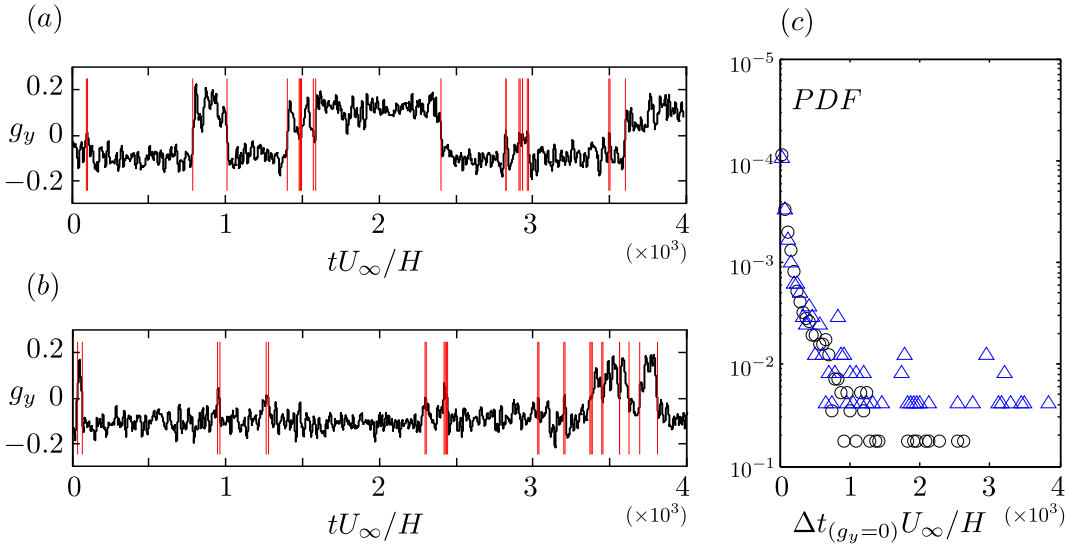

Figure 4. Time series of the horizontal component of the pressure gradient g_y for the body aligned with the flow $\beta = 0°$ in (a) and with the yaw $\beta = -2°$ in (b). Each vertical red segment in (a, b) indicates an event $g_y = 0$ with sign change. Waiting times statistics (c) between two consecutive events $g_y = 0$ for $\beta = 0°$ (black circles) and $\beta = -2°$ (blue triangles).

displayed as dashed lines in Fig. 5. They retrieve very satisfactorily the tails of the PDF and provide unambiguously a measure of the turbulent gradient fluctuation of each state given by their standard deviation denoted σ_N and σ_P. We can see that these fluctuations are not equal for the misaligned body in Fig. 5(b), but reduced for the predominant state and increased for the other in comparison to the aligned case in Fig. 5(a).

The Gaussian fits displayed by dashed lines in Fig. 5 are used to estimate the contribution κ of the local turbulent fluctuations to the zero pressure gradient realizations that are not associated with state changes. This contribution is given by the ratio at $g_y = 0$ of the Gaussian fits sum, $G(g_y)$ (continuous line in Fig. 5) to the PDF (red circles), say $\kappa = \frac{G(g_y=0)}{PDF(g_y=0)}$. Hence, in Fig. 5($a$), this contribution is 10% for the aligned body against 18% in Fig. 5(b) with yaw. It may be concluded that a non negligible part of the zero pressure gradient events are related to local random fluctuations. However, the rate of zero gradient events "really" associated with switching between the states can be evaluated from :

$$\mathcal{N}_s = (1-\kappa)\mathcal{N}_{(g_y=0)} \tag{1}$$

3.2. *Free-stream turbulence effect on switching statistics*

Figure 6 shows the horizontal pressure gradient statistics for the two free-stream turbulent intensities varying the yaw angle. At first glance, changing the turbulent intensity by a factor of about 3 produces only very little differences on the pressure gradient statistics. There is not much change either in the first statistical moments in Fig. 7(a). The variance $\overline{g_y^2} = \overline{g_y}^2 + \sigma_{g_y}^2$, giving a measure of the permanent asymmetry [15] is slightly increased with the larger turbulent intensity for almost all yaws. We also recover the results that the asymmetry of each state is constant, and independent of residual asymmetries introduced by the small yaws [16]. The turbulent intensity actually affects the yaw range on which the bistable dynamics occur. Bi-stability is associated with

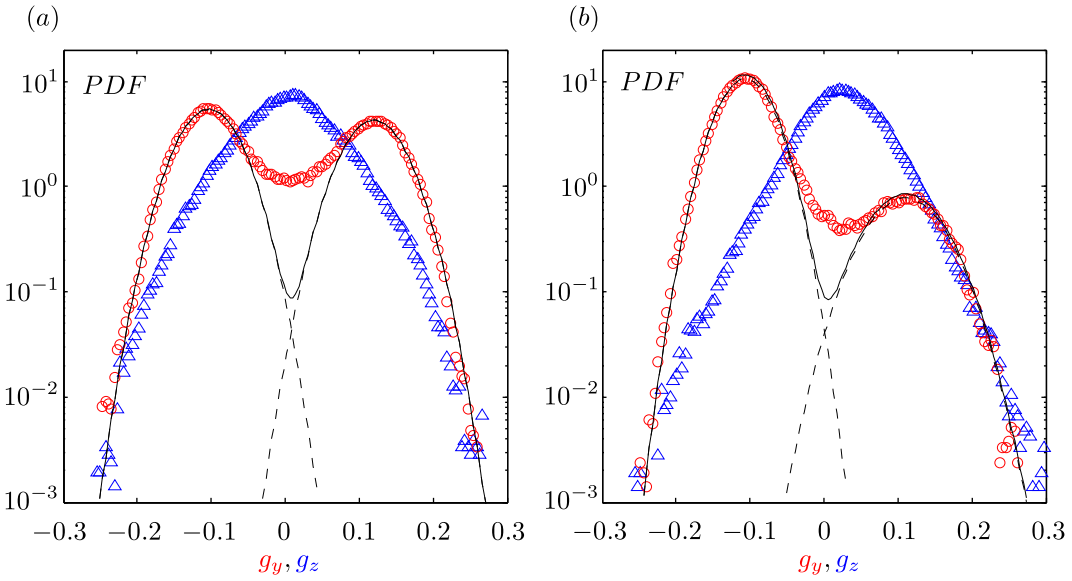

Figure 5. Probability density function (PDF) of the horizontal component of the pressure gradient g_y (red circles) and vertical component g_z (blue triangles) for the body aligned with the flow $\beta = 0°$ in (a) and with the yaw $\beta = -2°$ in (b). Dashed lines are Gaussian best fits centred on the most probable values of the PDF. The function $G(g_y)$ displayed with continuous lines is the sum of the two fitted Gaussian statistics and represents the contribution of random fluctuation not associated with wake state change.

high standard deviation σ_{g_y}, and the bistable yaw range given by the width of $\sigma_{g_y}(\beta)$ is smaller for larger turbulent intensity. As a consequence, the mean gradient $\overline{g_y}$ is more sensitive (steeper slope) to the yaw for the larger turbulent intensity. It can be noticed that for the higher turbulence intensity, the maximum of fluctuations is shifted towards negative yaw values. This is likely to be due to a modification of the incoming flow with the grid.

The effect of the free-stream turbulent intensity can be seen more clearly in Fig. 7(b) showing the turbulent fluctuation around each of the states, σ_P and σ_N as determined in § 3.1. It is shown that turbulent fluctuations around each state are significantly decreased when the free-stream turbulent intensity is increased. This surprising result indicates that the incoming flow fluctuations are not directly related to the wake fluctuations. We can also observe that independently to the turbulent intensity, the predominant state is always the one with the lowest fluctuations.

Finally, the rate at which the wake changes state is first assessed by the switching rate of zero horizontal pressure gradient events $\mathcal{N}_{(g_y=0)}$ in Fig. 8(a). The rate is significantly decreased on the whole range of yaws when the turbulent intensity is increased. However, we show in Fig. 8(b), the switching rate $\mathcal{N}_s$ corrected following Eq. 1 in order to remove events that do not correspond to a global wake switch. Indeed, as reported in Fig. 7(b), the reduction of the turbulent fluctuation around each of the states due to the increase of the turbulent intensity irremediably decreases the number of zero gradient realizations. The quantity $\mathcal{N}_s$ should then better assess the rate of wake state change from the local pressure measurements. Despite the reduction of the switching rate observed with the lower free-stream intensity in Fig. 8(b), we still obtain a significant decrease of the wake switching of about 35% overall the whole yaw range for the larger free-stream turbulent intensity.

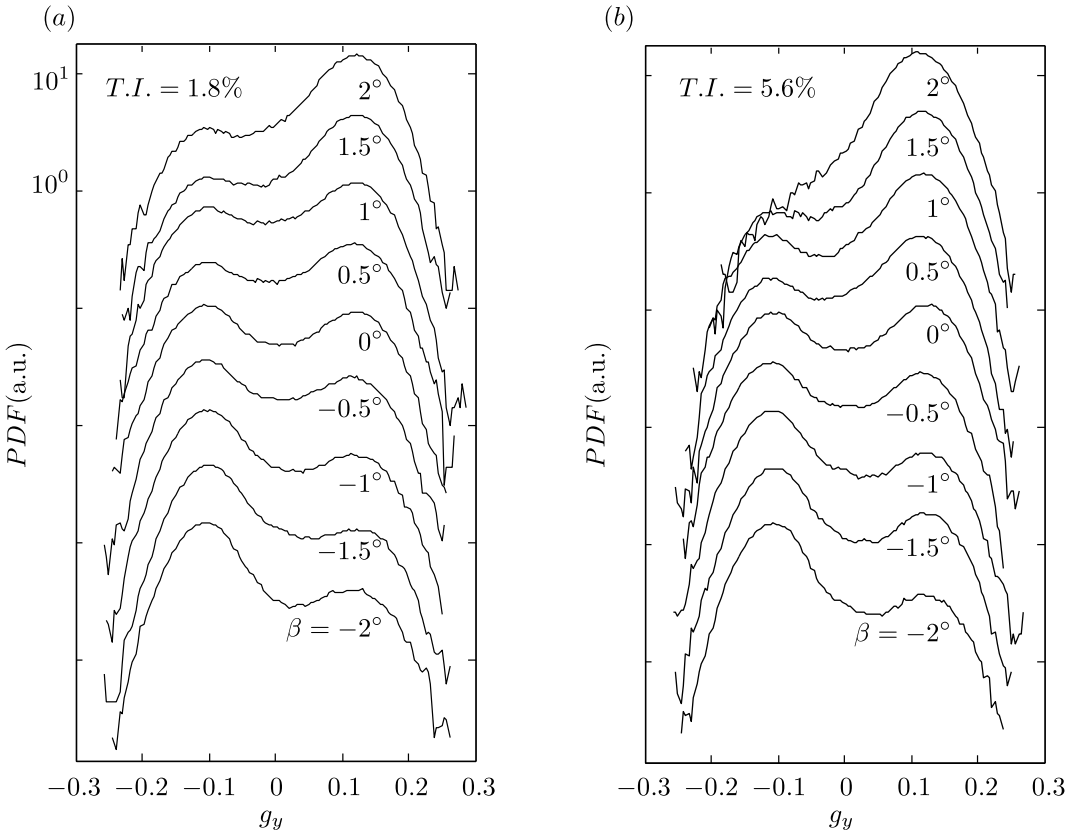

Figure 6. Probability density function (PDF) of the horizontal component of the pressure gradient g_y varying the body yaw from $\beta = -2°$ to $\beta = 2°$ by step of 0.5° with a free-stream turbulent intensity of 1.8% in (a) and 5.6% in (b).

4. Discussion and conclusion

The present experimental investigation addressed the question of how does the free-stream turbulent intensity modify the state switching dynamics. The difficulty is to assess, from few local pressure measurements subjected to turbulent fluctuations if a switching implying the whole wake structure has occurred. A technique is proposed, leading to the result that the switching rate is decreased as the turbulent intensity is increased independently to residual asymmetries. In addition, it is found that the fluctuation around each of the states is also decreased, but that the asymmetry intensity and the wake sensitivity to the residual asymmetry are reinforced. Our observations are totally consistent with the stochastic model presented in [10, 11] providing that the random fluctuation is associated with the turbulent motion produced by the wake instability and not introduced by the incoming flow. Coming back to the analogy with buckling, the periodic shedding (i.e. major unsteady instability of the wake) would be sufficient to produce random switching of the wake (no need for stochastic forcing) as in the beam experiment of [9]. This idea of chaotic dynamics in a turbulent context was explored in [17] and a recent numerical simulation proposed that large hairpin vortices are responsible for the triggering of the switching [18].

The question of why large free-stream turbulent intensity reduces turbulent motions of the wake is explained by a thickening of the boundary layers that develop on the body leading to thicker unstable free shear layers aft the body. As accordingly reported by [19] for circular cylin-

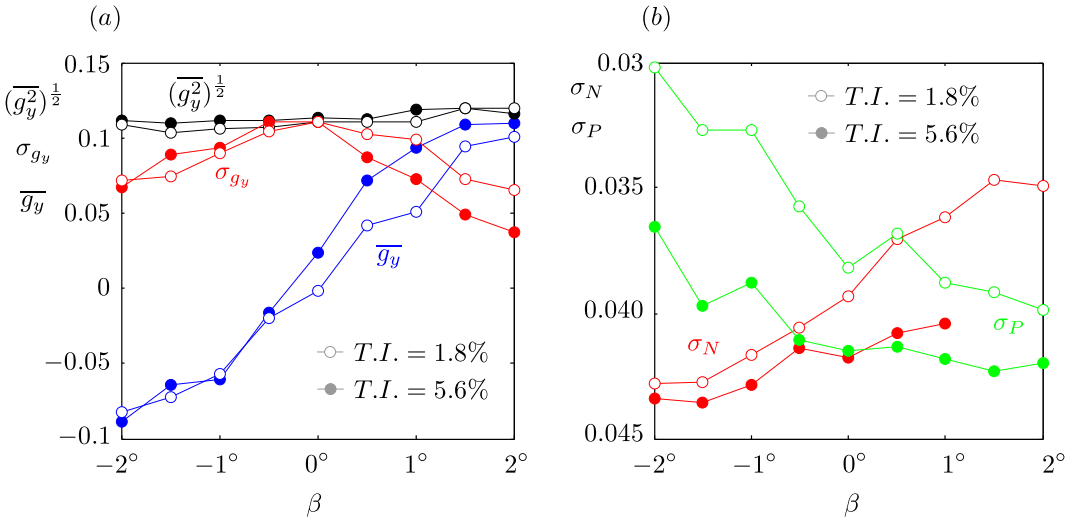

Figure 7. Square root of the variance of the horizontal pressure gradient component $(\overline{g_y^2})^{\frac{1}{2}}$ and its decomposition into fluctuations σ_{g_y} and average $\overline{g_y}$ (*a*) vs. the yaw. Standard deviations (*b*) of the random fluctuation (see text) about the state *N* (red) and *P* (green) vs. the yaw. In (*a*) and (*b*) empty symbols denote the lower free-stream turbulent intensity and filled symbols the larger turbulent intensity.

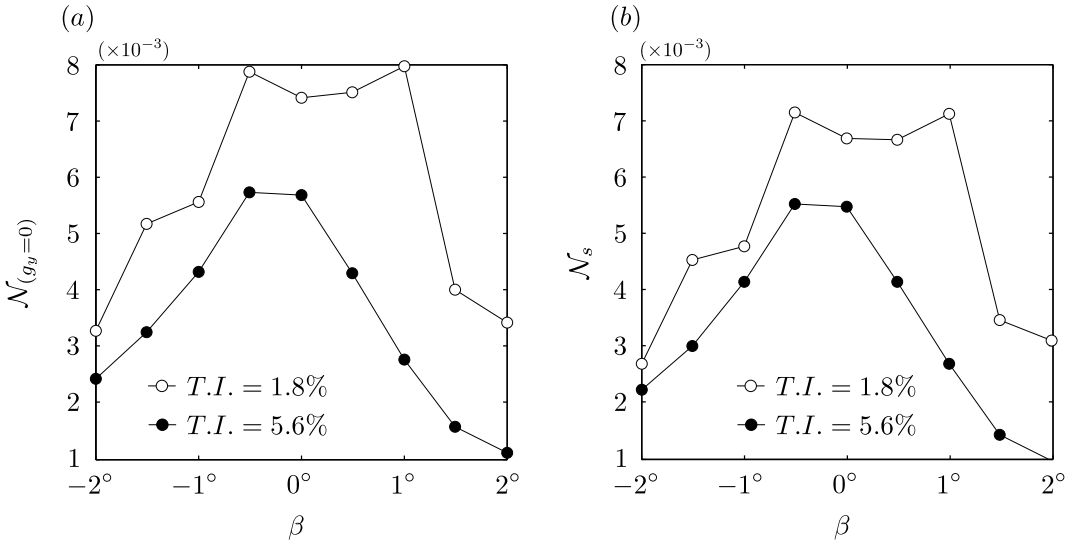

Figure 8. Switching rate in non-dimensional time unit computed (*a*) from the zero pressure gradient events statistics as shown in Fig. 4 and weighted (*b*) by the proportion of state change evaluated from Eq. 1.

ders, a high turbulent level of the free-stream decreases significantly the Strouhal number of vortex shedding compared to that of a low turbulence level as a consequence of the free-shear layers thickening.

Acknowledgements
The authors are grateful to Prof Cyril Touzé for useful discussions on buckling dynamics and to John R. Wrightson for his contribution to the manuscript. This work has been supported by the Khalifa University of Science and Technology under Award No. CIRA-2019-025.

References

[1] S. Douady, Y. Couder, "Phyllotaxis as a physical self-organized growth process", *Physical Review Letters* **68** (1992), no. 13, p. 2098-2101.
[2] Y. Couder, L. Pauchard, C. Allain, M. Adda-Bedia, S. Douady, "The leaf venation as formed in a tensorial field", *European Physical Journal B* **28** (2002), no. 2, p. 135-138.
[3] Y. Couder, E. Fort, "Single-particle diffraction and interference at a macroscopic scale", *Physical Review Letters* **97** (2006), no. 15, p. 154101.
[4] A. Eddi, E. Fort, F. Moisy, Y. Couder, "Unpredictable tunneling of a classical wave-particle association", *Physical Review Letters* **102** (2009), no. 24, p. 240401.
[5] M. Grandemange, M. Gohlke, O. Cadot, "Reflectional symmetry breaking of the separated flow over three-dimensional bluff bodies", *Physical Review E* **86** (2012), p. 035302.
[6] G. Bonnavion, O. Cadot, V. Herbert, S. Parpais, R. Vigneron, J. Délery, "Asymmetry and global instability of real minivans' wake", *Journal of Wind Engineering and Industrial Aerodynamics* **184** (2019), p. 77-89.
[7] D. Fabre, F. Auguste, J. Magnaudet, "Bifurcations and symmetry breaking in the wake of axisymmetric bodies", *Physics of Fluids* **20** (2008), p. 051702.
[8] D. Ormières, M. Provansal, "Transition to turbulence in the wake of a sphere", *Physical Review Letters* **83** (1999), no. 1, p. 80-83.
[9] F. Moon, P. Holmes, "A magnetoelastic strange attractor", *Journal of Sound and Vibration* **65** (1979), no. 2, p. 275-296.
[10] G. Rigas, A. Morgans, R. D. Brackston, J. Morrison, "Diffusive dynamics and stochastic models of turbulent axisymmetric wakes", *Journal of Fluid Mechanics* **778** (2015), p. R2.
[11] R. D. Brackston, J. García De La Cruz, A. Wynn, G. Rigas, J. F. Morrison, "Stochastic modelling and feedback control of bistability in a turbulent bluff body wake", *Journal of Fluid Mechanics* **802** (2016), p. 726–749.
[12] S. Ahmed, G. Ramm, G. Faitin, "Some salient features of the time-averaged ground vehicle wake", *SAE Technical Paper Series* (1984), p. 840300.
[13] M. Grandemange, M. Gohlke, O. Cadot, "Turbulent wake past a three-dimensional blunt body. Part 1. Global modes and bi-stability.", *Journal of Fluid Mechanics* **722** (2013), p. 51-84.
[14] M. Kiya, Y. Abe, "Turbulent elliptic wakes", *Journal of Fluids and Structures* **13** (1999), no. 7-8, p. 1041-1067.
[15] M. Grandemange, M. Gohlke, O. Cadot, "Turbulent wake past a three-dimensional blunt body. Part 2. Experimental sensitivity analysis.", *Journal of Fluid Mechanics* **752** (2014), p. 439-461.
[16] G. Bonnavion, O. Cadot, "Unstable wake dynamics of rectangular flat-backed bluff bodies with inclination and ground proximity", *Journal of Fluid Mechanics* **854** (2018), p. 196-232.
[17] E. Varon, Y. Eulalie, S. Edwige, P. Gilotte, J.-L. Aider, "Chaotic dynamics of large-scale structures in a turbulent wake", *Physical Review Fluids* **2** (2017), p. 034604.
[18] L. Dalla Longa, O. Evstafyeva, A. Morgans, "Simulations of the bi-modal wake past three-dimensional blunt bluff bodies", *Journal of Fluid Mechanics* **866** (2019), p. 791-809.
[19] J. Gerrard, "The mechanics of the formation region of vortices behind bluff bodies", *Journal of Fluid Mechanics* **25** (1966), no. 02, p. 401-413.